This article has been accepted for publication in a future issue of this journal, but has not been fully edited. Content may change prior to final publication. Citation information: DOI 10.1109/TPWRS.2018.2824823, IEEE Transactions on Power Systems

Analytical Method to Aggregate Multi-Machine SFR Model with Applications in Power System Dynamic Studies

Qingxin Shi, *Student Member, IEEE*; Fangxing Li, *Fellow, IEEE*; Hantao Cui, *Student Member, IEEE*

***Abstract*—The system frequency response (SFR) model describes the average network frequency response after a disturbance and has been applied to a wide variety of dynamic studies. However, the traditional literature does not provide a generic, analytical method for obtaining the SFR model parameters when the system contains multiple generators; instead, a numerical simulation-based approach or the operators' experience are the common practice to obtain an aggregated model. In this paper, an analytical method is proposed for aggregating the multi-machine SFR model into a single-machine model. The verification study indicates that the proposed aggregated SFR model can accurately represent the multi-machine SFR model. Furthermore, the detailed system simulation illustrates that the SFR model can also accurately represent the average frequency response of large systems for power system dynamic studies. Finally, three applications of the proposed method are explored, with system frequency control, frequency stability, and dynamic model reduction. The results show the method is promising with broad potential applications.**

***Index Terms*--System frequency response (SFR), multi-machine, frequency control, demand response, renewable energy penetration, model reduction.**

I. Introduction

Power system frequency stability can be challenged by such significant disturbances as a generator unit trip, a sudden heavy load change, or a system islanding event that is caused by a tie-line trip [1]. Following such disturbances, the system frequency experiences a drop, reaches the nadir and then enters a new equilibrium point (f_{nep}) below the nominal value (i.e., 60Hz). During this process, there are several indices for describing the dynamic performance of a system, including the frequency nadir (f_{nadir}), time to reach frequency nadir (t_{nadir}), and rate of change of frequency (RoCoF).

A low-order system frequency response (SFR) model was proposed in [2]. The model represents the average response of all generators following a load-generation unbalance. However, it is not clarified how to compute the equivalent model parameters if the system consists of multiple machines with heterogeneous parameters. It is true that system identification (SI) is a useful approach if the high-resolution frequency response data is available; also, numerical simulation studies and operators' experience can be applied to obtain the parameters [3]-[4]. However, since the number of integrated generators is always changing due to unit-commitment, the computation workload will be extremely high if we use the system identification method many times. In other words, there is a lack of analytical method for aggregating multi-machines to a single-machine SFR model with high accuracy, which is the initial motivation of this research work.

On the other hand, the SFR model can be applied to a wide variety of studies related to power system dynamics.

1) *Demand response for frequency control:* Reference [5]-[6] evaluated the impact of under-frequency load shedding (UFLS) on the frequency response based on a multi-machine SFR (MM-SFR) model. Compared with a severe disturbance that triggers the UFLS, frequency control strategies deal with smaller frequency disturbances. It was proposed that demand response (DR) participate in frequency regulation [7]-[13]. Based on the MM-SFR model, a state-space equation was established and a robust control algorithm was adopted to optimize the frequency response [11]. In a system with many generators, however, the state-space equation is of high order due to a large number of machines. This situation challenges the implementation of the frequency regulation algorithms because online computation is required.
2) *Frequency stability analysis:* In recent years, some conventional generators are replaced by renewable energy sources, which lower the system mechanical inertia and capability of frequency regulation [14]-[17]. In particular, with the same amount of generation outage, f_{nadir} will be lower and closer to the UFLS threshold [18]. The maximum renewable energy source (RES) penetration should be determined based on the system frequency security criterion [19]. The SFR model can provide a fast and straightforward tool for conducting this study.
3) *Coherency-based dynamic model reduction*: In the industry application, the power utilities usually employ the reduced model instead of the full model for dynamic security assessment. For instance, the widely-used 179-bus Western Electricity Coordinating Council (WECC) system is reduced from the original 10,000+ bus transmission system based on the concept of coherency and generator aggregation. The dynamic model reduction

This work was supported by the Engineering Research Center Program of the National Science Foundation and the Department of Energy of USA under NSF Award Number EEC-1041877 and the CURENT Industry Partnership Program.

Q. Shi, F. Li, and H. Cui are with Department of Electrical Engineering and Computer Science, the University of Tennessee, Knoxville. TN 37996, USA (Emails: qshi1@vols.utk.edu; fli6@utk.edu; hcui7@vols.utk.edu. Corresponding author: F. Li).

This article has been accepted for publication in a future issue of this journal, but has not been fully edited. Content may change prior to final publication. Citation information: DOI 10.1109/TPWRS.2018.2824823, IEEE Transactions on Power Systems

involves the aggregation of turbine governors. The proposed method is an effective tool for this task.

To summarize, we desire to aggregate the MM-SFR model into a single-machine model, which is called an *aggregated SFR* (ASFR) *model*. Then, it is very convenient for us to implement the above studies.

In addition, SFR is a simplification of the detailed power system model, which consists of exciters, synchronous generators, network topology, and ZIP loads. Therefore, it is reasonable that the frequency output of the SFR model has some error. First, the inter-machine frequency oscillation exists in the multi-machine system [20]. Second, the exciter's voltage control and voltage-dependent loads can also affect frequency response [21]. Due to these factors, the frequency response of the SFR model has some error if compared with that of the detailed system model, which has not been thoroughly discussed in the previous works such as [2] and [22]. It is necessary to conduct a comprehensive analysis on the accuracy of the SFR model for representing the detailed system. This also provides the theoretical foundation for the aforementioned research topics.

Based on the above discussions and motivations, this paper proposes an ASFR model and verifies it by large-scale system simulation. The model is an extension of [2] and helpful in power system dynamic studies.

The remaining parts of this paper are organized as follows. Section II reviews the problem of inter-machine oscillation, which affects the local bus frequency response. Section III describes the time-domain response of the SFR model. Section IV proposes the ASFR model and proves it mathematically. Section V verifies the model by transfer function simulation and detailed system simulation, respectively. Section VI provides three examples to illustrate the application of the model. Finally, a conclusion is made in Section VII.

II. Description of Inter-Machine Oscillation

This section provides an overview of the inter-machine oscillation, which describes the dynamic behaviors of multiple generators that are caused by a sudden system's power unbalance. The theory is described in [20]. An understanding of this theory is helpful to evaluate the accuracy of the ASFR model that is proposed in later Sections.

At any instant, the electric power produced by the generators should be equal to the power consumed by the load. When a disturbance (e.g., a large generator outage) occurs, the power unbalance is formed between generation and network consumption. However, the RoCoF of each generator is not identical because each one covers different portions of the power unbalance.

A. Swing Equation of a Single Machine

Consider a single-machine system in which the exciter is neglected. The rotating speed of the generator follows the 2nd Newton Law. Applying small deviations around the nominal frequency, we have [1]:

$$2H\frac{d\Delta f(t)}{dt} = P_m(t) - P_d(t) = \Delta P_m(t) - \Delta P_d(t) \tag{1}$$

where $P_m(t)$ is the generator mechanical power, $P_d(t)$ is the load demand, and $\Delta f(t)$ is the system frequency deviation ($=f(t)–f_{rated}$), all at time t. Here, the power and frequency variables are in per-unit values. H is the inertia constant, representing the kinetic energy at the rated speed divided by the rated power base. If we assume the pre-disturbance state as the steady state, then the accelerating power ($P_m–P_d$) equals to the difference between the generation and demand power deviations from the steady state ($\Delta P_m–\Delta P_d$).

B. Equivalent Parameter of Multi-machine System

In the multi-machine system, the frequency response of each generator is not necessarily identical. Therefore, to derive a swing equation for the system, we should define an equivalent generator that reflects the average behavior of all the generators. This generator is called the center of inertia (COI) [23]. According to the definition of the inertia constant, the individual inertia constant w.r.t. the system rated power is

$$H_{i,sys} = H_i \cdot \left(S_i \Big/ \sum_{j=1}^{N} S_j \right) = H_i \cdot \left(S_i / S_{sys} \right) \tag{2}$$

where S_i is the rated apparent power of the generator #i, and S_{sys} is the sum of the system installed generation capacity:

$$S_{sys} = \sum_{j=1}^{N} S_j \tag{3}$$

By applying the procedure that is given in [20], the COI frequency (f_{COI}) is given as follows [23]-[24]:

$$f_{COI} = \left(\sum_{i=1}^{N} f_i H_{i,sys} \right) \Big/ \left(\sum_{i=1}^{N} H_{i,sys} \right) \tag{4}$$

C. Power Unbalance at $t = 0^+$

Immediately after the moment of the disturbance (at $t=0^+$), the turbine governor control has not yet taken effect. The power unbalance is distributed among the generators according to their synchronizing power coefficients (P_{sij}) [20]. As is shown in Fig. 1, at $t = 0$, the disturbance ΔP_L at Bus k causes a change of the voltage phasor at Bus i. Then,

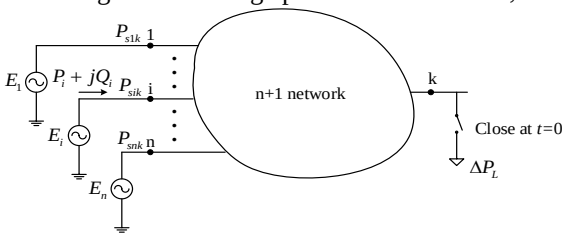

Fig. 1. Network with power unbalance at bus k [20].

$$\Delta P_{di}(0^+) = \left(P_{sik} \Big/ \sum_{j=1}^{N} P_{sjk} \right) \cdot \Delta P_L \tag{5}$$

where $\Delta P_{di}(0^+)$ is the power unbalance share of generator i. P_{sik} is defined as

$$P_{sik} = V_i V_k (B_{ik} \cos\delta_{ik0} - G_{ik} \sin\delta_{ik0}) \tag{6}$$

where V_i and V_k are the voltage magnitude of bus i and k, respectively. B_{ik} and G_{ik} are the real and imaginary parts of the admittance between bus i and k. δ_{ik0} is the pre-disturbance angle difference between bus i and k. For each generator, substituting (5) into (1), we can find the initial RoCoF [20]:

This article has been accepted for publication in a future issue of this journal, but has not been fully edited. Content may change prior to final publication. Citation information: DOI 10.1109/TPWRS.2018.2824823, IEEE Transactions on Power Systems

$$2H_i \frac{d\Delta f_i(0^+)}{dt} = -\Delta P_{di}(0^+) \tag{7}$$

According to (6), the machines that have smaller electrical distance from the point of disturbance will pick up the greater share of the power unbalance ΔP_L. Consequently, the closer generators will have larger RoCoF at the instant the disturbance occurs.

D. Oscillation and Power Unbalance after $t = 0^+$

During a very short period after $t=0^+$, the impact of the turbine governor control is negligible. Each generator shares ΔP_{sys} according to its inertia. Then, the share of power unbalance is determined by (8) [20]:

$$\Delta P_{di}(t) = \left(H_i \Big/ \sum_{i=1}^{N} H_i \right) \cdot \Delta P_L \tag{8}$$

For a generator, $\Delta P_{di}(t)$ is not necessarily equal to $\Delta P_{di}(0^+)$ because its P_{sik} and H_i may take different portions of the entire system parameter. Thus, right after 0^+, the power unbalance share of generator i gradually changes from $\Delta P_{di}(0^+)$ to $\Delta P_{di}(t)$. In this process, the generators may exchange real power with each other, which is called inter-machine oscillation [25]. After several seconds, the oscillation decays and the frequency at all buses gradually becomes identical [20].

III. Single-machine SFR Model

The complete SFR model is presented in Fig. 2 (a). The parameters are listed in TABLE I. Since T_G and T_C are much smaller than T_R, we can simplify the SFR model by neglecting these two parts [2]. Then, the low-order SFR model is shown in Fig. 2 (b). The frequency deviation, Δf (= $f - f_{rated}$), in the time domain is given by (9) [2]:

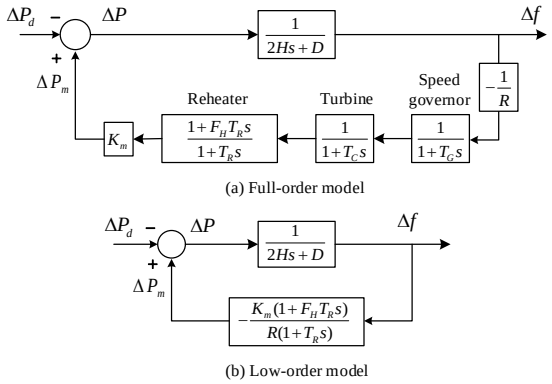

Fig. 2. Single-machine SFR transfer function model.

TABLE I: Typical Ranges of FR Model Parameters [1], [2], [26].

Parameter	Typical value
Governor time constant T_G	0.15~0.3 s
Steam chest time constant T_C	0.2~0.5 s
Reheat time constant T_R	6~14 s
High-pressure turbine fraction F_H	0.15~0.4
Inertia constant H	3~9 s
Governor speed regulation R	0.04~0.1
Load damping factor D	0~2%

$$\Delta f(t) = \frac{R\Delta P}{DR+1} \cdot \left[1 + \alpha e^{-\zeta \omega_n t} \sin\left(\omega_r t + \varphi \right) \right] \tag{9}$$

where the natural oscillation frequency ω_n, the damping ratio ζ, the damped frequency ω_r, and coefficients α, φ are calculated from the SFR model parameters, which can be found in [2]. Then, the frequency derivative is obtained:

$$f'(t) = \frac{d\Delta f(t)}{dt} = -\frac{R\Delta P}{DR+1} \cdot \alpha \omega_n e^{-\zeta \omega_n t} \sin\left(\omega_r t + \varphi_1 \right) \tag{10}$$

At the frequency nadir, the derivative of the frequency curve should be 0, as shown in Fig. 3. In other words, at f_{nadir}, we should have the very first instance of $f'(t) = 0$. Therefore, t_{nadir} can be solved by

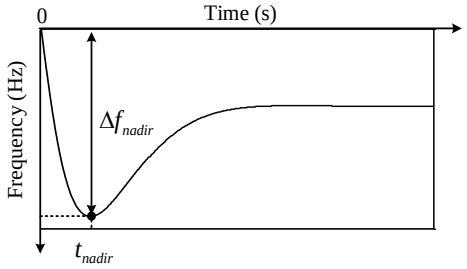

Fig. 3. Frequency response after step disturbance.

$$t_{nadir} = \frac{1}{\omega_r} \tan^{-1} \left(\frac{\omega_r T_R}{\varsigma \omega_n T_R - 1} \right) \tag{11}$$

Thus, substituting (11) to (9) gives the frequency deviation. Since $\Delta f_{nadir} = f_{nadir} - f_{rated}$, we have

$$\Delta f_{nadir} = \frac{R\Delta P}{DR+1} \cdot \left[1 + \sqrt{1-\varsigma^2}\, \alpha e^{-\zeta \omega_n t_{nadir}} \right] \tag{12}$$

Therefore, the frequency nadir can be calculated by (12) instead of performing the time-domain simulation. It clearly indicates that Δf_{nadir} is proportional to ΔP. In a practical system, however, the premise of making use of (10)-(12) is that the multiple machines with various parameters can be aggregated to a single machine.

IV. Analytical Method to Aggregate SFR Model

Based on the works in [2], this section demonstrates how to aggregate the MM-SFR model to the ASFR model. The method is validated by the mathematical proof.

A. Formulation of ASFR Model

In Fig. 4 (a), the droop value R_i is correlated to S_i (after reaching the steady state, $\Delta P_{mi}=S_i \cdot \Delta f/R_i$). Also, the multiple turbine governors are summed up with a constant gain $K_{mi}=S_i/S_{sys}$, which represents the portion of rated power of machine i w.r.t. the whole system. The equivalent droop value R is given by (13) [1]:

$$\frac{1}{R} = \sum_{i=1}^{N} \frac{K_{mi}}{R_i} = \sum_{i=1}^{N} \kappa_i \tag{13}$$

where the equivalent gain is defined as $\kappa_i=K_{mi}/R_i$. In the ASFR model (shown in Fig. 4 (b)), the four equivalent parameters (T_G, T_C, T_R and F_H) represent the combined effect of N turbine governors. To simplify the description, we define the normalized gain λ_i of each branch in Fig. 4 (a).

$$\lambda_i = \kappa_i \Big/ \sum_{i=1}^{N} \kappa_i \tag{14}$$

$$\sum_{i=1}^{N} \lambda_i = 1 \tag{15}$$

This article has been accepted for publication in a future issue of this journal, but has not been fully edited. Content may change prior to final publication. Citation information: DOI 10.1109/TPWRS.2018.2824823, IEEE Transactions on Power Systems

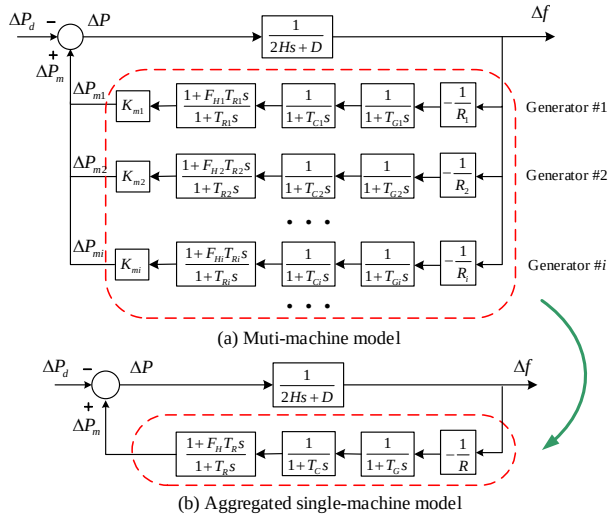

Fig. 4. Aggregation of SFR model.

According to the red dashed blanket in Fig. 4, the transfer function of a single machine can represent that of multiple machines. Then, (16) can be deducted (the detail is presented in Appendix A).

$$\sum_{i=1}^{N}\lambda_i\frac{1+F_{Hi}T_{Ri}s}{(1+T_{Gi}s)(1+T_{Ci}s)(1+T_{Ri}s)}=\frac{1+F_HT_Rs}{(1+T_Gs)(1+T_Cs)(1+T_Rs)} \tag{16}$$

Traditionally, the parameters $X=\{T_G,\ T_C,\ F_H,\ T_R\}$ can be obtained by SI [3]. The principle of SI is to find the optimal X, with the objective that the equivalent machine output approximates the output of all machines as closely as possible, if the same Δf is input [3]. This paper, however, proposes an analytical method for calculating X. Since a larger λ_i value means that generator #i has a larger rated power and more sensitive frequency droop, it has a larger impact on the equivalent X. Therefore, it is reasonable to guess that the ASFR model parameters equal to the weighted average of those of each machine:

$$X=\sum_{i=1}^{N}\lambda_iX_i \tag{17}$$

The following sections will prove that the ASFR model parameters can be calculated by (17) with high accuracy.

To simplify the proof work, the transfer function is split into two parts with proper coefficients A_R and A_G. It can be verified in Appendix B that any error of this representation is not significant:

$$\frac{1+F_{Hi}T_{Ri}s}{(1+T_{Gi}s)(1+T_{Ci}s)(1+T_{Ri}s)}\approx\frac{A_R(1+F_{Hi}T_{Ri}s)}{1+T_{Ri}s}+\frac{A_G}{(1+T_{Gi}s)(1+T_{Ci}s)} \tag{18}$$

Therefore, (16) is also split into equations, given by (19) and (20). We only need to prove that both of the two equations are valid.

$$\sum_{i=1}^{N}\lambda_i\frac{1+F_{Hi}T_{Ri}s}{1+T_{Ri}s}=\frac{1+F_HT_Rs}{1+T_Rs} \tag{19}$$

$$\sum_{i=1}^{N}\lambda_i\frac{1}{(1+T_{Gi}s)(1+T_{Ci}s)}=\frac{1}{(1+T_Gs)(1+T_Cs)} \tag{20}$$

B. Mathematical Validation

In this paper, (19) and (20) are proven by the *mathematical induction method*, which consists of two steps.

1) Two-machine case: The first step is to consider the simplest case, N=2. The problem is formulated as: proving the magnitudes of the error function $e_R(s)$ and $e_G(s)$ are negligible, where $e_R(s)$ is defined as

$$e_R(s)=\lambda_1\frac{1+F_{H1}T_{R1}s}{1+T_{R1}s}+\lambda_2\frac{1+F_{H2}T_{R2}s}{1+T_{R2}s}-\frac{1+F_HT_Rs}{1+T_Rs}=\frac{P_R(s)}{Q_R(s)} \tag{21}$$

where

$$\frac{P_R(s)}{Q_R(s)}=\frac{a_3s^3+a_2s^2+a_1s+a_0}{b_3s^3+b_2s^2+b_1s+b_0} \tag{22}$$

Similarly, $e_G(s)$ is defined as

$$e_G(s)=\lambda_1\frac{1}{1+T_{G1}s}+\lambda_2\frac{1}{1+T_{G2}s}-\frac{1}{1+T_Gs}=\frac{P_G(s)}{Q_G(s)} \tag{23}$$

where

$$\frac{P_G(s)}{Q_G(s)}=\frac{c_2s^2+c_1s+c_0}{d_3s^3+d_2s^2+d_1s+d_0} \tag{24}$$

First, we analyze the frequency characteristic of $e_R(s)$. Expanding $P_R(s)$ gives the expression of polynomial coefficients a_i (i = 0, 1, 2, 3). Based on (15) and (17) in N = 2 case, we can simplify the expression of a_i. The detailed deduction is presented in Appendix C. Then, we have

$$a_0=a_3=0 \tag{25}$$

Two non-zero terms are a_1 and a_2. Although they depend on the turbine governor parameters, we can determine their upper bound and compare them with b_1 and b_2.

$$a_1=\lambda_1\lambda_2(F_{H1}-F_{H2})(T_{R1}-T_{R2}) \tag{26}$$

Obviously, $|a_1|$ is proportional to two terms $|F_{H1}–F_{H2}|$ and $|T_{R1}–T_{R2}|$. Since

$$\lambda_1\lambda_2\le\left(\frac{\lambda_1+\lambda_2}{2}\right)^2=0.25$$

The upper bound of $|a_1|$ is determined:

$$\begin{aligned}|a_1|&=|\lambda_1\lambda_2(F_{H1}-F_{H2})(T_{R1}-T_{R2})|\\&\le 0.25\cdot|0.4-0.15|\cdot|14-6|\\&=0.5\end{aligned} \tag{27}$$

The expression of a_2 is the most complex one. We can determine its upper-bound by amplifying the expression:

$$a_2\le 0.25\cdot(T_{R1}-T_{R2})^2=0.25\cdot(14-6)^2=16 \tag{28}$$

Expanding $Q_R(s)$ gives the expression of polynomial coefficients b_i (i = 0, 1, 2, 3).

$$\begin{aligned}b_3&=T_{R1}T_{R2}T_R\\b_2&=T_{R1}T_R+T_{R2}T_R+T_{R1}T_{R2}\\b_1&=T_{R1}+T_{R2}+T_R\\b_0&=1\end{aligned} \tag{29}$$

Equations (27)-(29) indicate that a_1, a_2 are more sensitive with $|F_{H1}–F_{H2}|$ and $|T_{R1}–T_{R2}|$ than b_1, b_2. Therefore, the "worst case" that maximizes the ratios $|a_1/b_1|$ and $|a_2/b_2|$ is: λ_1=λ_2=0.5, meanwhile $|F_{H1}–F_{H2}|$ and $|T_{R1}–T_{R2}|$ reaches the maximum. For example, T_{R1}=14, T_{R2}=6, and F_{H1}=0.4, F_{H2}=0.15. Then, we

This article has been accepted for publication in a future issue of this journal, but has not been fully edited. Content may change prior to final publication. Citation information: DOI 10.1109/TPWRS.2018.2824823, IEEE Transactions on Power Systems

have T_R=10 and F_H=0.28. The ratios can be estimated.

$$\left|\frac{a_1}{b_1}\right| \le \frac{0.5}{6+14+10} = 0.025 \tag{30}$$

$$\left|\frac{a_2}{b_2}\right| \le \frac{16}{6\cdot 14+6\cdot 10+14\cdot 10} = 0.056 \tag{31}$$

Equations (30) and (31) indicate that the magnitude of the error function is much smaller than 1. Define the per-unit error function $e_{R,pu}(s)$, which means the error of ΔP_m when the ASFR model is applied.

$$e_{R,pu}(s) = \frac{e_R(s)}{\Delta P_m(s)} = \frac{e_R(s)}{\lambda_1 \dfrac{1+F_{H1}T_{R1}s}{1+T_{R1}s} + \lambda_2 \dfrac{1+F_{H2}T_{R2}s}{1+T_{R2}s}} \tag{32}$$

Let $s=j\omega$, where ω is the oscillation frequency in rad/s. The frequency characteristic of $e_{R,pu}(s)$ is calculated for discrete values of frequency from 0.01-1Hz, as presented in Fig. 5. The damped frequency ω_r of the SFR model is usually less than 0.5rad/s (≈0.08Hz) [2]. Therefore, the magnitude of $e_{R,pu}(s)$ is less than 5.5% according to Fig. 5. However, the magnitude of $e_{R,pu}(s)$ will significantly decrease if $|F_{H1}–F_{H2}|$ and $|T_{R1}–T_{R2}|$ become smaller. Therefore, the "N=2" case of (19) is proven.

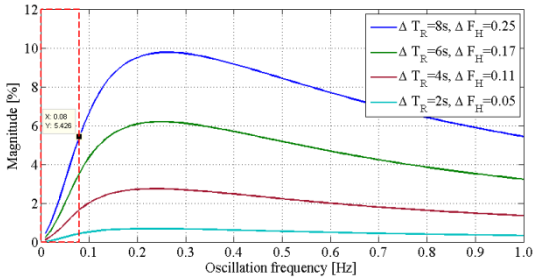

Fig. 5. Frequency characteristic of $e_{R,pu}(s)$.

Second, we analyze the frequency characteristic of $e_G(s)$ in a similar way. In $P_G(s)$, the only non-zeros term is c_2. The upper bound is

$$\begin{aligned}\left|\frac{c_2}{d_2}\right| &\le \frac{0.25(T_{G1}-T_{G2})^2}{T_{G1}T_{G2}+T_{G1}T_G+T_{G2}T_G} \\ &< \frac{0.25\cdot(0.15-0.3)^2}{0.15\cdot 0.3+0.15\cdot 0.225+0.3\cdot 0.225} \\ &= 0.038\end{aligned} \tag{33}$$

Therefore, we can approximate the upper bound of the error function $|e_G(s)|$ is determined by $|T_{G1}–T_{G2}|$. Then, the following equation is proven:

$$\lambda_1 \frac{1}{1+T_{G1}s} + \lambda_2 \frac{1}{1+T_{G2}s} = \frac{1}{1+T_G s} \tag{34}$$

Similarly, we have

$$\lambda_1 \frac{1}{1+T_{C1}s} + \lambda_2 \frac{1}{1+T_{C2}s} = \frac{1}{1+T_C s} \tag{35}$$

Since the transfer function of two series-connected inertia elements is a linear combination of them, given by (36), equation (20) is also proven.

$$\frac{1}{(1+T_G s)(1+T_C s)} = \frac{1}{T_G - T_C}\left(\frac{T_G}{1+T_G s} - \frac{T_C}{1+T_C s}\right) \tag{36}$$

Based on the above analysis, (17) is finally proven for the "N=2" case.

2) Multi-machine case: The second step is to prove the multiple-machine case. The main idea is to "merge" the machines one by one. Here we take the parameter T_R as an example for illustrating the method. As is shown in Fig. 6, assume the former k machines can be aggregated into an equivalent machine:

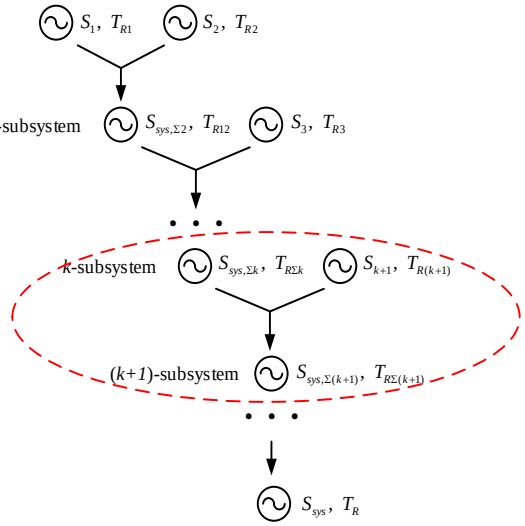

Fig. 6. Flowchart of aggregating the time constant.

$$T_{R,\Sigma k} = \sum_{i=1}^{k} \lambda_i T_{Ri} = \sum_{i=1}^{k} \frac{\kappa_i}{\kappa_{\Sigma k}} T_{Ri} \tag{37}$$

Then, we aim to prove that the (k+1)-th machine can also be merged into this equivalent machine:

$$T_{R,\Sigma(k+1)} = \sum_{i=1}^{k+1} \lambda_i T_{Ri} = \sum_{i=1}^{k} \frac{\kappa_i}{\kappa_{\Sigma(k+1)}} T_{Ri} \tag{38}$$

If a system consists of N machines, we assume having merged k (k<N) machines as a k-th equivalent machine. If we consider this as the "k-subsystem" of the entire system, then the subsystem base power is defined as

$$\kappa_{\Sigma k} = \sum_{i=1}^{k} \kappa_i \tag{39}$$

If the (k+1)-th machine is merged, the resulting "(k+1)-subsystem" consists of two parts: the previous k-subsystem and the (k+1)-th machine, shown in the red dashed circle of Fig. 6. Then, the base power of the (k+1)-subsystem is updated. The equivalent gain κ_i w.r.t. the (k+1)-subsystem is determined as

$$\begin{aligned}\lambda_{\Sigma k} &= \frac{\kappa_{\Sigma k}}{\kappa_{\Sigma(k+1)}} = \frac{\kappa_{\Sigma k}}{\kappa_{\Sigma k}+\kappa_{k+1}} \\ \lambda_{k+1} &= \frac{\kappa_{k+1}}{\kappa_{\Sigma(k+1)}} = \frac{\kappa_{k+1}}{\kappa_{\Sigma k}+\kappa_{k+1}}\end{aligned} \tag{40}$$

Based on (40), the equivalent reheat time constant of the (k+1)-subsystem can be deducted:

This article has been accepted for publication in a future issue of this journal, but has not been fully edited. Content may change prior to final publication. Citation information: DOI 10.1109/TPWRS.2018.2824823, IEEE Transactions on Power Systems

$$
\begin{aligned}
T_{R,\Sigma(k+1)} &= \lambda_{\Sigma k} T_{R,\Sigma k} + \lambda_{k+1} T_{R(k+1)} \\
&= \frac{\kappa_{\Sigma k}}{\kappa_{\Sigma k}+\kappa_{k+1}} \sum_{i=1}^{k} \lambda_i T_{Ri} + \frac{\kappa_{k+1}}{\kappa_{\Sigma k}+\kappa_{k+1}} T_{R(k+1)} \\
&= \frac{\kappa_{\Sigma k}}{\kappa_{\Sigma k}+\kappa_{k+1}} \sum_{i=1}^{k} \left(\frac{\kappa_i}{\kappa_{\Sigma k}} T_{Ri} \right) + \frac{\kappa_{k+1}}{\kappa_{\Sigma k}+\kappa_{k+1}} T_{R(k+1)} \\
&= \sum_{i=1}^{k} \left(\frac{\kappa_i}{\kappa_{\Sigma k}+\kappa_{k+1}} T_{Ri} \right) + \frac{\kappa_{k+1}}{\kappa_{\Sigma k}+\kappa_{k+1}} T_{R(k+1)} \\
&= \sum_{i=1}^{k+1} \left(\frac{\kappa_i}{\kappa_{\Sigma(k+1)}} T_{Ri} \right) \\
&= \sum_{i=1}^{k+1} \lambda_i T_{Ri}
\end{aligned}
\tag{41}
$$

Follow similar steps until k+1=N, and all the machines are merged into one equivalent machine. Therefore, (17) is proven for any N value because it can satisfy (16) with considerable accuracy. In the same way, other parameters F_H, T_G and T_C in the ASFR model can be proven.

Admittedly, each merging step can cause some error. After many steps of merging, we have $\lambda_{\Sigma k} >> \lambda_{k+1}$. According to (27) and (28), a_1 and a_2 will be very small and $X_{R(k+1)}$ will not fluctuate much in each merging step. Then, the accumulative error will finally converge. Although it is impossible to accurately estimate the upper-bound of the error, this section provides a method to illustrate which is the "worst case" that results in the maximal ΔP_m error. In the next section, the maximal error can be simulated to verify the accuracy of the proposed model.

C. Discussions on the SFR Model

The SFR model is mainly based on the turbine governor control, which modifies the mechanical power output of the prime mover according to the rotor-angle speed deviation. Overall, the SFR model extracts the turbine governor and frequency-dependent load from the detailed power system. It neglects those elements that do not directly affect the generator mechanical power output, including the exciter, synchronous generator, and voltage-dependent loads. The SFR model can be used to analyze the dynamic behavior of multi-machine systems. However, it should be noticed that there are some intrinsic limitations in the SFR model because the following factors are neglected:

- *The turbine governor nonlinearity*: The traditional SFR model is an idealized model which ignores the frequency deadband and maximal turbine governor response. In North America, the frequency deadband is ±0.03 or ±0.04Hz and the maximal response is usually 6% of the generator rated power [27]. For some generators, the percentage of maximal response can be higher due to the operators' setting [28]. Thus, we can add a limiter to the SFR model at the ΔP_m output terminal if a more accurate simulation result is needed.
- *The inter-machine oscillation*: In the MM-SFR model, all the turbine governors are preserved while the inertia constants are aggregated [2]. Also, the network model is ignored. Therefore, the SFR can only represent the average system frequency because the frequency oscillation depends on both the network topology and each generator's inertia constant.
- *The impact of a voltage-dependent load*: The power unbalance causes not only a frequency deviation but also a voltage deviation. These two deviations in turn affect the power consumption of frequency- and voltage-dependent loads. Therefore, neglecting the voltage-dependent load brings a little error to the frequency [21].
- *The impact of network loss variation*: The network loss may also change after a disturbance. Then, ΔP_L slightly differs from the generator outage or load increase amount. Consequently, f_{nep} value output by the SFR model is slightly different from f_{nep} output by detailed system model.

Based on the above limitations, it can be expected that the dynamic frequency generated by the SFR model may have a little error from the detailed system model, both in a dynamic state and in a steady state. The next section will evaluate through simulation studies whether the errors are significant.

V. Simulation Study

The performance of the proposed model is verified in this section. The simulation study will compare three dynamic models, which are named Level 1, 2 and 3, according to the degree of simplification:

- *ASFR model* (*Level 1*): includes an aggregated turbine governor element and the total inertia;
- *MM-SFR model* (*Level 2*): includes turbine governor element and the total inertia;
- *Detailed system model* (*Level 3*): includes network topology, turbine governor, exciter, and synchronous generator.

The SFR model is simulated by the Matlab-Simulink with a time step of 0.01s, while the detailed system is simulated by the Matlab-based PSAT software package [29].

A. ASFR Model v.s. MM-SFR Model

The MM-SFR and ASFR model are shown in Fig. 4 (a) and Fig. 4 (b), respectively. In this subsection, we verify the proposed aggregation method by simulating a 6-machine system. Since the model parameters X can be any values within the normal range (listed in TABLE I), we should simulate the worst case that maximizes the frequency nadir error. If a system contains a large number of generators, the distribution pattern of X can be classified into three cases:

Case 1 (Parameter evenly distributed): The parameters are listed in Table II.

Case 2 (Parameter saddleback-shaped distributed): The X value of most machines are close to its upper bound or lower bound. The parameters of a 6-machine system are listed in Table III. For example, the T_R value is either close to 6s or to 14s.

Case 3 (Parameter olive-shaped distributed): The X value of most machines is close to the average value. According to the analysis in Section IV(B), Case 3 is not the worst case because X is in a more narrow range than the other two cases. Thus, the simulation of Case 3 is neglected.

In the bottom row of TABLE II and Table III, the equivalent

This article has been accepted for publication in a future issue of this journal, but has not been fully edited. Content may change prior to final publication. Citation information: DOI 10.1109/TPWRS.2018.2824823, IEEE Transactions on Power Systems

parameters are calculated by equations (13), (14), (17). In addition, the practical prime movers are classified as a "with reheater" type and a "no reheater" type, which are adopted by different literatures [11], [13]. In this subsection, we set all T_R and F_H to 0 when simulating the "no reheater" type.

In simulation Case 1, we apply a step disturbance of ΔP= $0.05S_{sys}$ to the 6-machine system and obtain the frequency deviation and mechanical power deviation. Note: the ΔP_m curve of MM-SFR model is the sum of 6 generators. Fig. 7 is the comparison of "with reheater" SFR models. Fig. 8 is the comparison of "no reheater" SFR models.

TABLE II. PARAMETERS OF 6-MACHINE SFR MODEL-CASE 1*.

Gen. No.	K_m	T_G (s)	T_C (s)	T_R (s)	F_H (pu)	1/R	λ
1	0.14	0.20	0.37	10.5	0.28	13.33	0.113
2	0.18	0.12	0.24	9	0.17	10	0.109
3	0.19	0.27	0.41	6	0.23	20	0.230
4	0.22	0.30	0.48	14	0.32	16.67	0.222
5	0.14	0.22	0.36	12	0.39	20	0.169
6	0.13	0.19	0.21	8.5	0.24	20	0.157
Equ.	1.00	0.231	0.363	10.0	0.278	16.5	1.00

* H=4.96s, D=1.2.

TABLE III. PARAMETERS OF 6-MACHINE SFR MODEL-CASE 2*.

Gen. No.	K_m	T_G (s)	T_C (s)	T_R (s)	F_H (pu)	1/R	λ
1	0.14	0.16	0.27	6	0.19	13.33	0.113
2	0.18	0.19	0.23	7.5	0.17	10	0.109
3	0.19	0.17	0.22	6.5	0.22	20	0.230
4	0.22	0.24	0.42	12	0.39	16.67	0.222
5	0.14	0.26	0.49	14	0.36	20	0.169
6	0.13	0.29	0.46	13.5	0.35	20	0.157
Equ.	1.00	0.221	0.355	10.1	0.293	16.5	1.00

* H=4.96s, D=1.2.

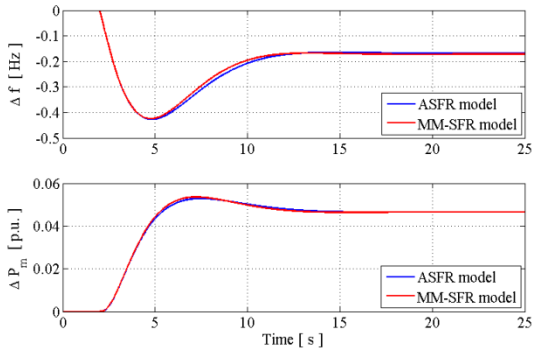

Fig. 7. Frequency & generation response of ASFR model of Case 1 (with reheater model).

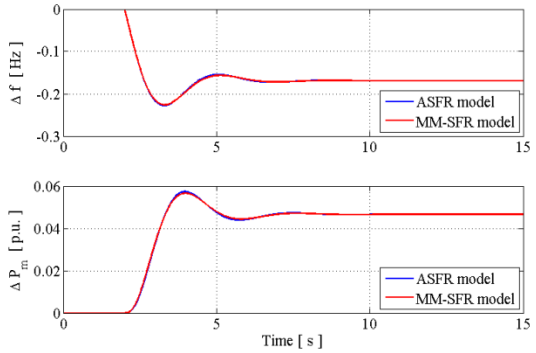

Fig. 8. Frequency & generation responses of ASFR model of Case 1 (non-reheater model).

The same simulation is done for Case 2. The relative errors of Δf_{nadir} and t_{nadir} are defined as

$$err_f = \frac{\Delta \hat{f}_{nadir} - \Delta f_{nadir}}{|\Delta f_{nadir}|} \times 100 \quad (42)$$

$$err_t = \frac{\hat{t}_{nadir} - t_{nadir}}{t_{nadir}} \times 100 \quad (43)$$

where the head sign means the value is estimated by the ASFR model. It should be noticed that the above relative error remains constant when ΔP changes because of the linearity of inverse Laplace Transformation [30]. The frequency nadir errors are summarized in Table IV, which indicates that the error in Case 2 is slightly higher than in Case 1. However, the frequency nadir errors are generally very small even for the two worst cases ($|err_f|$<1% and $|err_t|$<2%). Then, we can conclude that the errors of all other cases are almost within this threshold. Based on the mathematical proof in Section IV and the simulation study of a "bad" case, we can conclude that the ASFR model can replace the MM-SFR model with high accuracy.

TABLE IV. ERROR SUMMARY OF SIMULATION CASES.

Types	With reheater		Non-reheater	
	err_f	err_t	err_f	err_t
Case 1	-0.77%	1.26%	-0.75%	-0.33%
Case 2	-0.89%	1.71%	-0.95%	-0.36%

In addition, some references [2], [22] claim that T_G and T_C can be neglected in the SFR model ("with reheater" type) due to their small values. A simulation study between low-order and full-order SFR model is done with the parameters in TABLE II. As is shown in Fig. 9, the low-order model results in a err_f of more than 10%. Therefore, the low-order SFR model is more suitable for analytical and qualitative studies.

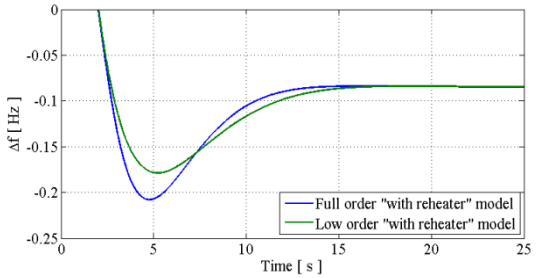

Fig. 9. Frequency response of full-order and low-order SFR model.

B. ASFR Model vs. Small-Scale Detailed System Model

The SFR model is compared with an IEEE 14-bus, 5 machine system, as shown in Fig. 10. The turbine governor parameters are listed in TABLE V. We still apply a sudden load increase of ΔP=$0.05S_{sys}$ to both models. The computation time of the ASFR model is less than 0.5s, while that of the detailed model is 33s.

Scenario 1: As is presented in Fig. 11 (a), the frequency response curves obtained by the two models are quite close. The relative errors are err_f = -4.41% and err_t = 5.27%, respectively. Right after the disturbance, the frequency responses of the separate buses are slightly different (shown in the dashed green blanket), which is caused by the inter-machine oscillation. Besides, there is a 3.35% (0.0028Hz) error with Δf_{nep}. According to the discussion in Subsection IV.C, the system power loss can increase slightly after the

This article has been accepted for publication in a future issue of this journal, but has not been fully edited. Content may change prior to final publication. Citation information: DOI 10.1109/TPWRS.2018.2824823, IEEE Transactions on Power Systems

sudden load increase of $0.05S_{sys}$, and the equivalent ΔP in the ASFR model should be slightly larger than "0.05p.u.". Since we still take ΔP=0.05p.u. in the ASFR model, the resulting f_{nep} is slightly higher than f_{nep} in the detailed system model.

Scenario 2: We further verify the accuracy of ASFR model by including DR. The first case shows a load reduction of $0.03S_{sys}$ is activated at 2.8s, while the second case shows the same load reduction is activated at 4.0s. The results of both cases are presented in Fig. 11 (b). Based on the two scenarios, the factors (discussed in Subsection IV.C) do not have significant impact on the accuracy of the ASFR model.

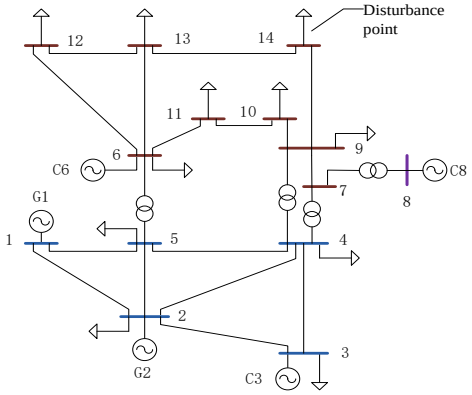

Fig. 10. IEEE 14-bus testing system.

TABLE V. PARAMETERS OF 5 TURBINE GOVERNORS.

Gen. No.	K_m	T_G (s)	T_C (s)	T_R (s)	F_H (pu)	$1/R$	λ
1	0.469	0.2	0.33	10	0.23	25	0.564
2	0.25	0.13	0.25	12	0.21	20	0.240
3	0.188	0.22	0.26	14	0.35	12.5	0.113
4	0.047	0.24	0.37	8	0.29	16.7	0.038
5	0.047	0.18	0.25	9	0.2	20	0.045
Equiv.	1.00	0.186	0.301	10.8	0.240	20.8	1.00

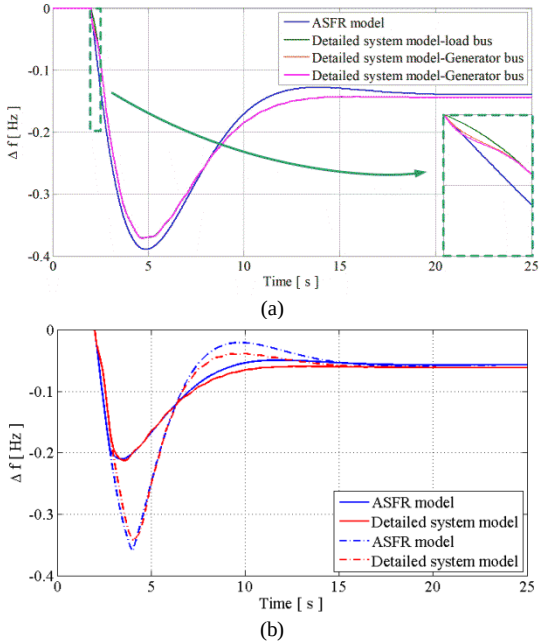

Fig. 11. Frequency response of ASFR model and IEEE 14-bus detailed system: (a) without DR; (b) with DR.

C. ASFR Model v.s. Large-scale Detailed System Model

In this subsection, a 179-bus, 29-machine U.S. simplified WECC system is simulated. The geographic diagram of the testing system is shown in Fig. 12. In this system, the system base power S_{sys} is 130.5GVA, and the total loading level is 60.9GW. The distribution of two parameters (T_R, F_H) of 29 machines is plotted in Fig. 13. In this large system, we can divide the T_R-F_H plane into nine sub-regions. In each sub-region, since T_R and F_H are within a narrow range of 3s and 0.1 (as the dashed line shows), respectively, the merging error is negligible according to (27) and (28). Then, we can expect that no matter how many machines are aggregated, the indices err_f and err_t will not be obviously larger than the 6-machine system.

Fig. 12. WECC 179-bus testing system.

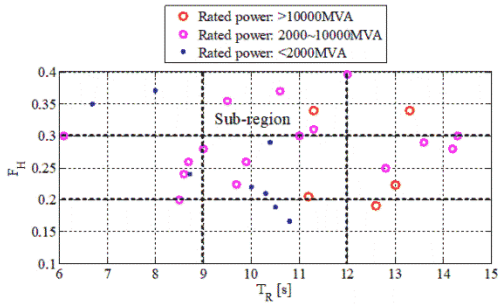

Fig. 13. Distribution of turbine governor parameters.

We apply a sudden load increase of $0.2\%S_{sys}$ at a bus near Los Angeles and observe the frequency response of three representative load buses according to their distance from Los Angeles: Los Angeles (nearby), Phoenix (medium), and Portland (far). Meanwhile, the equivalent parameters are fed into the ASFR model. The frequency responses of two models are presented in Fig. 14. We have the following observations.

- As is shown in Fig. 14 (a), the frequency responses at different buses have significant difference. At further buses, the frequency drops more slowly after the disturbance, because the remote generators have a smaller share of power unbalance at the time instant t=0$^+$, according to the discussion in Subsection II.C. Therefore,

This article has been accepted for publication in a future issue of this journal, but has not been fully edited. Content may change prior to final publication. Citation information: DOI 10.1109/TPWRS.2018.2824823, IEEE Transactions on Power Systems

the large system has more significant inter-machine oscillations.

- In a large-scale system, f_{COI} (calculated by (4)) is an essential index for evaluating the overall frequency response [18]. Fig. 14 (b) indicates that the ASFR model can also simulate f_{COI} of a large-scale system with high accuracy. The relative errors are err_f = -4.69% and err_t = 1.75%, respectively. Furthermore, the authors in [31] proposed a frequency-propagation-based method to estimate the local bus frequency from on COI frequency.

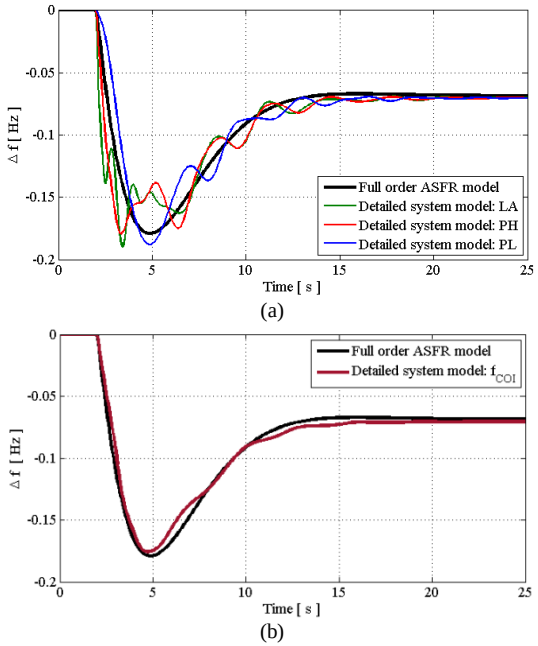

Fig. 14. Frequency response of ASFR model and 179-bus detailed system: (a) three typical bus frequency; (b) COI frequency.

D. A Summary of the ASFR Model

The SFR model extracts the turbine governor from the detailed power system and simulates its average frequency response. Based on the above analytical and simulation studies, different frequency response models and their relations are summarized in Fig. 15. The green arrow means this model simplification brings negligible error in frequency response, while the orange arrow means this model simplification perhaps brings considerable error. Among the six models, only the low-order ASFR model can give an analytical expression of the frequency nadir. This model is mainly applicable to two aspects of current studies: one is a qualitative analysis on frequency response features; the other is security-based unit commitment [22]. The full-order ASFR model can replace small-scale systems for quantitative study with an acceptable error, although it ignores the inter-machine oscillation. Also, it can represent the average frequency response of large-scale systems, which is critical in industry applications [18].

As is discussed in Section I, the ASFR model has applications in several research areas. When the size of the target system is not large, we can replace the detailed system with an ASFR model to obtain the parameters f_{nadir} and t_{nadir} with very low computation workload and satisfactory accuracy. For a large-scale system, however, the ASFR model is a fast tool for the researchers to find a rough estimate of f_{nadir} w.r.t. a specified ΔP. Then, the detailed system simulation is conducted to figure out the accurate value. Therefore, the ASFR model and detailed system model are complementary.

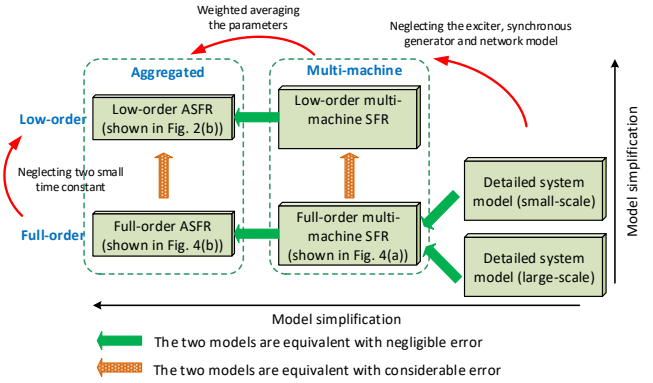

Fig. 15. Summary of different models for studying the frequency dynamic.

VI. Applications of ASFR Model

This section introduces three applications of the ASFR model.

A. Demand Response for Frequency Regulation

Subsection V.A concludes that the ASFR model (both "with reheater" and "no reheater" type) can replace the MM-SFR model with high accuracy. An enhanced version of the SFR model is called the "load frequency control" (LFC) model, which includes an automatic generation control (AGC) element $K(s)$. Many studies have been done on DR for frequency regulation [7]-[11]. Fig. 16 shows a single-area, 5-machine system, where α_i is the share of regulation amount. The state-space model for frequency control is given by (44) [7]:

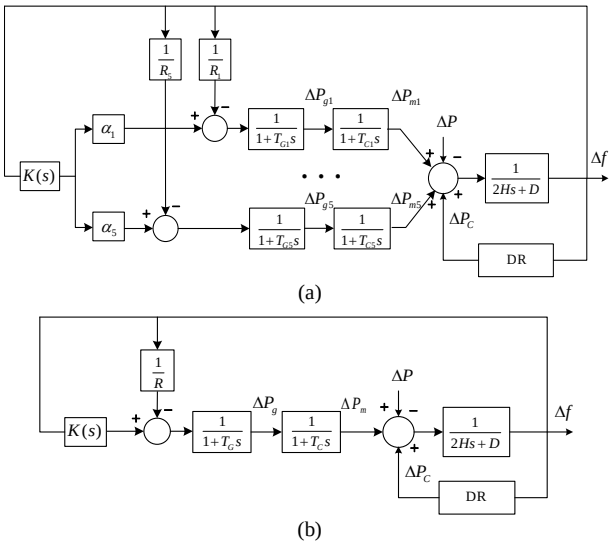

Fig. 16. Multi-machine LFC model with secondary frequency regulation: original model; (b) aggregated model.

$$\begin{aligned} \dot{\boldsymbol{x}} &= \boldsymbol{A}\boldsymbol{x} + \boldsymbol{B}\boldsymbol{u} + \boldsymbol{\Gamma}\boldsymbol{w} \\ \boldsymbol{y} &= \boldsymbol{C}\boldsymbol{x} \end{aligned} \tag{44}$$

In a conventional approach, the state vector $\boldsymbol{x}$ is 11-order: $\boldsymbol{x}=[\Delta f, \Delta P_{m1}, \ldots \Delta P_{m5}, \Delta P_{g1}, \ldots \Delta P_{g5}]^T$. The expressions of $\boldsymbol{A}$, $\boldsymbol{B}$, $\boldsymbol{C}$ and $\boldsymbol{\Gamma}$ are also 11-order and omitted here due to space

This article has been accepted for publication in a future issue of this journal, but has not been fully edited. Content may change prior to final publication. Citation information: DOI 10.1109/TPWRS.2018.2824823, IEEE Transactions on Power Systems

limitations. Based on the ASFR model, we can merge the five machines into one machine and $\boldsymbol{x}$ is reduced to 3-order:

$$\boldsymbol{A}=\begin{bmatrix} -\frac{D}{2H} & \frac{1}{2H} & 0 \\ 0 & -\frac{1}{T_C} & \frac{1}{T_C} \\ -\frac{1}{T_G R} & 0 & -\frac{1}{T_G} \end{bmatrix},\ \boldsymbol{B}=\begin{bmatrix} \frac{\mu-1}{2H\mu} \\ 0 \\ \frac{1}{T_G} \end{bmatrix},\ \boldsymbol{\Gamma}=\begin{bmatrix} -\frac{1}{2H} \\ 0 \\ 0 \end{bmatrix}$$

$$\boldsymbol{C}=\begin{bmatrix}1,0,0\end{bmatrix},\ \boldsymbol{x}=\begin{bmatrix}\Delta f, \Delta P_m, \Delta P_g\end{bmatrix}^T,\ \boldsymbol{u}=\Delta P_S,\ \boldsymbol{w}=\Delta P,$$

$$\boldsymbol{y}=\Delta f\ .$$

where μ ($0<\mu<1$) is the share of DR in total frequency regulation effort, and μ=0.1 in this case. The turbine governor parameters are shown in Table II. The linear quadratic regulator (LQR) algorithm is applied to optimize the frequency response. After a disturbance of ΔP=0.025p.u., the control strategies based on the ASFR and MM-SFR models achieve very close frequency responses, as shown in Fig. 17. Furthermore, the ASFR model is also applicable to multi-area frequency regulation problems [11], in which each area can be aggregated to a single machine.

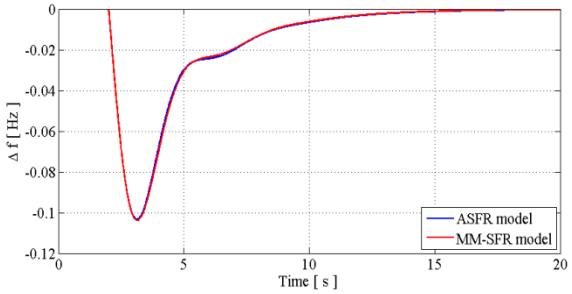

Fig. 17. Comparison between MM-SFR model and ASFR model.

B. Estimation of Maximal Renewable Energy Penetration

The maximal RES penetration is generally determined based on several frequency security criteria, such as f_{nadir}, f_{nep} and a 15-second rolling window [19]. The ASFR model provides a fast technique for this study, which is useful in power planning and generation dispatch [17]-[18], [32].

The RES penetration mainly affects the system total inertia and frequency regulation reserve. Traditional wind generators contribute much less to the system inertia and frequency droop than the same capacity of synchronous generators [15], [33]-[34]. In recent years, however, it is proposed that wind turbines can utilize the DC-link capacitor energy and rotor kinetic energy to provide system inertia support [35]. With this control scheme, wind generators can contribute more to the system inertia. Assuming that the fraction of inertia that wind power contributes to the system is k_w, the fraction of synchronous generator inertia that is reduced in the presence of wind is k_s (normally $k_w<k_s$). The new inertia constant and speed droop is calculated by (45) and (46) [15]:

$$H_{sys,new}=H_{sys,old}(1+k_w-k_s) \tag{45}$$

$$R_{sys,new}=\frac{R_{sys,old}}{1+k_w-k_s} \tag{46}$$

Besides, the equivalent turbine parameters should also be recalculated by (13), (14), and (17) because part of the synchronous generators are replaced by wind generators. This model can also be extended to multi-area system. The system frequency response can be simulated after substituting the new parameters to the SFR or LFC model. For instance, the authors in [15] concluded that the frequency deviation, the tie-line power flow and the area control error tend to increase.

C. Coherency-based Power System Model Reduction

The system dynamic model reduction technique is based on coherency. Coherency means that some synchronous generators, which are usually close to each other, exhibit similar frequency responses and rotor angle swings after a disturbance. The overall procedure for forming coherency-based dynamic equivalents can be divided into two main steps. The first step is to identify groups of coherent generators in the study area. The second is to aggregate each coherent group of machines into a single equivalent machine, followed by eliminating unnecessary generator/load buses. The machine aggregation includes turbine governors, exciters and synchronous generators. The detail of the model reduction technique is discussed in [3].

Based on the accuracy of the ASFR model that is verified in Section V, the proposed weighted-average method can be used to aggregate multiple turbine governors that are identified as coherent. Therefore, this method is an essential addition to the existing technique of power system model reduction. For instance, the full WECC system consists of about 18,000 buses. The aforementioned WECC 179-bus system is an example of the reduced order model, which is normally used in online dynamic security assessment [3].

VII. Conclusions

This paper proposes an analytical method for obtaining the ASFR model parameters based on individual generator parameters.

- The first contribution is to propose an analytical method by which we can aggregate the MM-SFR model with high accuracy. The model is proven by a mathematical induction method and further verified by simulation studies.
- The second contribution is the investigation of the accuracy of the ASFR model for replacing the detailed system model. It can be concluded from dynamic simulation studies that the ASFR model can accurately represent the bus frequency response of a small-scale system. In a large-scale system, the ASFR model is less accurate for the bus frequency but can still represent the COI frequency accurately. Therefore, as a fast calculation tool, the ASFR model can support the studies related to power system dynamics.
- Last but not least, the applications of the proposed method are demonstrated with three studies: frequency regulation via DR, maximal wind power penetration, and dynamic model reduction. This shows the promising potentials to apply the proposed method in other related research.

This article has been accepted for publication in a future issue of this journal, but has not been fully edited. Content may change prior to final publication. Citation information: DOI 10.1109/TPWRS.2018.2824823, IEEE Transactions on Power Systems

VIII. Appendix

A. The Formulation of ASFR Model

According to the definition of the ASFR model (shown in Fig. 4), we have

$$\sum_{i=1}^{N}\left(K_{mi}\cdot\frac{1}{R_i}\cdot Gen_i(s)\right)=\frac{1}{R}\cdot Gen(s) \tag{47}$$

where

$$Gen(s)=\frac{1+F_H T_R s}{(1+T_G s)(1+T_C s)(1+T_R s)}$$

Substituting (13) to the right-hand side of (47) gives

$$\sum_{i=1}^{N}\left(\frac{K_{mi}}{R_i}\cdot Gen_i(s)\right)=\left(\sum_{i=1}^{N}\frac{K_{mi}}{R_i}\right)\cdot Gen(s) \tag{48}$$

Substituting (13) and (14) to (48) gives

$$\begin{aligned}\sum_{i=1}^{N}\left(\kappa_i\cdot Gen_i(s)\right)&=\left(\sum_{i=1}^{N}\kappa_i\right)\cdot Gen(s)\\ \sum_{i=1}^{N}\left(\left(\kappa_i\Big/\sum_{i=1}^{N}\kappa_i\right)\cdot Gen_i(s)\right)&=Gen(s)\\ \sum_{i=1}^{N}\left(\lambda_i\cdot Gen_i(s)\right)&=Gen(s)\end{aligned} \tag{49}$$

B. Linear Approximation of Turbine Governor Function

The right side of (18) can be expressed as a polynomial function:

$$\frac{A_R(1+F_{Hi}T_{Ri}s)}{1+T_{Ri}s}+\frac{A_G}{(1+T_{Gi}s)(1+T_{Ci}s)}=\frac{p_3s^3+p_2s^2+p_1s+p_0}{q_3s^3+q_2s^2+q_1s+q_0} \tag{50}$$

The coefficients of the right side of (50) are shown in Table VI.

Table VI. Coefficients of the transfer function.

i	p_i	q_i
3	$A_R F_{Hi}T_{Ri}T_{Gi}T_{Ci}$	$T_{Ri}T_{Gi}T_{Ci}$
2	$A_G(F_{Hi}T_{Ri}T_{Gi}+F_{Hi}T_{Ri}T_{Ci}+T_{Gi}T_{Ci})$	$T_{Ri}T_{Gi}+T_{Ri}T_{Ci}+T_{Ci}T_{Gi}$
1	$A_R(F_{Hi}T_{Ri}+T_{Gi}+T_{Ci})+A_G T_{Ri}$	$T_{Ri}+T_{Gi}+T_{Ci}$
0	A_R+A_G	1

Assume there exists a pair of A_R and A_G values that make the left and right side of (51) have an equal frequency characteristic:

$$\frac{p_3s^3+p_2s^2+p_1s+p_0}{q_3s^3+q_2s^2+q_1s+q_0}=\frac{F_{Hi}T_{Ri}s+1}{(1+T_{Gi}s)(1+T_{Ci}s)(1+T_{Ri}s)} \tag{51}$$

Let $p_1 = F_{Hi}T_{Ri}$ and $p_0 = 1$, and solve for

$$\begin{cases}A_R=\dfrac{(1-F_{Hi})T_{Ri}}{(1-F_{Hi})T_{Ri}+T_{Gi}+T_{Ci}}\approx 0.9\\ A_G=1-A_R\approx 0.1\end{cases} \tag{52}$$

Substituting (52) to the expression of other coefficients, we can conclude $p_3/q_3=A_RF_{Hi}<0.36$ and $p_2/q_2\approx A_GF_{Hi}<0.1$. Therefore, at the low-frequency band, the coefficients p_3 and p_2 can be neglected. Then, the approximated equation (18) is proved.

C. The Coefficients of the Error Function

The coefficients of $P_R(s)$ are deducted as follows:

$$a_0=\lambda_1+\lambda_2-1=0 \tag{53}$$

$$a_3=(\lambda_1F_{H1}+\lambda_2F_{H2}-F_H)T_{R1}T_{R2}T_R=0 \tag{54}$$

The expression of a_1 is simplified by substituting $\lambda_1+\lambda_2=1$ and $X=\lambda_1X_1+\lambda_2X_2$, respectively:

$$\begin{aligned}a_1&=\lambda_1(F_{H1}T_{R1}+T_{R2}+T_R)+\lambda_2(F_{H2}T_{R2}+T_{R1}+T_R)\\&\quad-(F_HT_R+T_{R1}+T_{R2})\\&=\lambda_1(1-\lambda_1)F_{H1}T_{R1}-\lambda_1\lambda_2(F_{H1}T_{R2}+F_{H2}T_{R1})+\lambda_2(1-\lambda_2)F_{H2}T_{R2}\\&=\lambda_1\lambda_2(F_{H1}T_{R1}-F_{H1}T_{R2}-F_{H2}T_{R1}+F_{H2}T_{R2})\\&=\lambda_1\lambda_2(F_{H1}-F_{H2})(T_{R1}-T_{R2})\end{aligned} \tag{55}$$

Similarly, the expression of a_2 is simplified. a_2 is amplified twice as follows:

$$\begin{aligned}a_2&=\lambda_1(F_{H1}T_{R1}T_{R2}+F_{H1}T_{R1}T_R+T_{R2}T_R)+\lambda_2(F_{H2}T_{R1}T_{R2}+\\&\quad F_{H2}T_{R2}T_R+T_{R1}T_R)-(F_HT_{R1}T_R+F_HT_{R2}T_R+T_{R1}T_{R2})\\&=\left[(\lambda_1T_{R2}+\lambda_2T_{R1})(\lambda_1T_{R1}+\lambda_2T_{R2})-T_{R1}T_{R2}\right]\\&\quad+\lambda_1\lambda_2(F_{H1}T_{R2}-F_{H2}T_{R1})(T_{R1}-T_{R2})\\&\le\left[\left(\frac{\lambda_1T_{R2}+\lambda_2T_{R1}+\lambda_1T_{R1}+\lambda_2T_{R2}}{2}\right)^2-T_{R1}T_{R2}\right]\\&\quad+\lambda_1\lambda_2(F_{H1}T_{R2}-F_{H2}T_{R1})(T_{R1}-T_{R2})\\&=\left[0.25\left((\lambda_1+\lambda_2)(T_{R1}+T_{R2})\right)^2-T_{R1}T_{R2}\right]\\&\quad+\lambda_1\lambda_2(F_{H1}T_{R2}-F_{H2}T_{R1})(T_{R1}-T_{R2})\\&\le 0.25\left[(T_{R1}-T_{R2})^2+(F_{H1}T_{R2}-F_{H2}T_{R1})(T_{R1}-T_{R2})\right]\end{aligned} \tag{56}$$

We can observe that the second term of a_2 reaches the maximum when T_{R1}=14s, T_{R2}=6s, F_{H1}=0.15s and F_{H2}=0.4s:

$$\begin{aligned}&\left|(F_{H1}T_{R2}-F_{H2}T_{R1})(T_{R1}-T_{R2})\right|\\&<\left|\frac{1}{F_{H2}T_{R2}^2}\left(\frac{F_{H1}}{F_{H2}}-\frac{T_{R1}}{T_{R2}}\right)\left(\frac{T_{R1}}{T_{R2}}-1\right)\right|\\&<\left|\frac{1}{0.4\times 6^2}\times\left(\frac{0.15}{0.4}-\frac{14}{6}\right)\times\left(\frac{14}{6}-1\right)\right|\\&<<(T_{R1}-T_{R2})^2\end{aligned}$$

Therefore, the upper bound of a_2 can be approximated as $0.25(T_{R1}-T_{R2})^2$.

IX. References

[1] P. Kundur, *Power system stability and control*, New York, NY, USA: McGraw-Hill, 1994.

[2] P. M. Anderson and M. Mirheydar, "A low-order system frequency response model," *IEEE Trans. Power Syst.*, vol. 5, pp. 720–729, Aug. 1990.

[3] J. Chow, *Power system coherency and model reduction*, Springer, 2013, pp. 33-35.

[4] S. H. Jakobsen and K. Uhlen, "Vector fitting for estimation of turbine governing system parameters," *2017 IEEE Manchester PowerTech*, Manchester, 2017, pp. 1-6.

[5] Denis Lee Hau Aik, "A general-order system frequency response model incorporating load shedding: analytic modeling and applications," *IEEE Trans. Power Syst.*, vol. 21, no. 2, pp. 709-717, May 2006.

[6] L. Sigrist, I. Egido and L. Rouco, "A method for the design of UFLS schemes of small isolated power systems," *IEEE Trans. Power Syst.*, vol. 27, no. 2, pp. 951-958, May 2012.

[7] S. A. Pourmousavi and M. H. Nehrir, “Introducing dynamic demand response in the LFC model,” *IEEE Trans. Power Syst.*, vol. 29, no. 4, pp. 1562-1572, Jul. 2014.
[8] Y. J. Kim, L. K. Norford and J. L. Kirtley, "Modeling and analysis of a variable speed heat pump for frequency regulation through direct load control," *IEEE Trans. Power Syst*, vol. 30, no. 1, pp. 397-408, Jan. 2015.
[9] L. Cai, Z. He and H. Hu, "A new load frequency control method of multi-area power system via the viewpoints of Port-Hamiltonian system and cascade system," *IEEE Trans. Power Syst.*, vol. 32, no. 3, pp. 1689-1700, May 2017.
[10] Q. Shi, H. Cui, F. Li, Y. Liu, W. Ju, and Y. Sun, “A hybrid dynamic demand control strategy for power system frequency regulation,” *CSEE J. Power Energy Syst.*, vol. 3, no. 2, pp. 17-26, Jun. 2017.
[11] J. Hu, J. Cao, J. M. Guerrero, T. Yong and J. Yu, "Improving frequency stability based on distributed control of multiple load aggregators," *IEEE Trans. Smart Grid*, vol. 8, no. 4, pp. 1553-1567, Jul. 2017.
[12] Q. Hu, F. Li, X. Fang, and L. Bai, "A framework of residential demand aggregation with financial incentives," *IEEE Trans. Smart Grid*, vol. 9, no. 1, pp. 497-505, Jan. 2018.
[13] Q. Shi, F. Li, Q. Hu, and Z. Wang, “Dynamic demand control for system frequency regulation: concept review, algorithm comparison, and future vision,” *Electr. Power Syst. Res.*, vol. 154, pp. 75-87, Jan. 2018.
[14] S. Liao, J. Xu, *et al*., "Load-damping characteristic control method in an isolated power system with industrial voltage-sensitive load," *IEEE Trans. Power Syst.*, vol. 31, no. 2, pp. 1118-1128, Mar. 2016.
[15] N. Nguyen and J. Mitra, "An analysis of the effects and dependency of wind power penetration on system frequency regulation," *IEEE Trans. Sustain. Energy*, vol. 7, no. 1, pp. 354-363, Jan. 2016.
[16] H. Pulgar-Painemal, Y. Wang, *et al.*, "On inertia distribution, inter-area oscillations and location of electronically-interfaced resources," *IEEE Trans. Power Syst.*, vol. 33, no. 1, pp. 995-1003, Jan. 2018.
[17] H. Yu, R. Bansal, and Z. Dong, “Fast computation of the maximum wind penetration based on frequency response in small isolated power systems,” *Applied Energy*, vol. 113, pp. 648-659, Jan. 2014.
[18] N. W. Miller, M. Shao, and S. Venkataraman, “California iso (CAISO) frequency response study,” General Elect. Int., Schenectady, NY, USA, Tech. Rep., 2011.
[19] H. Golpîra, H. Seifi, *et al.*, "Maximum penetration level of micro-grids in large scale power systems: frequency stability viewpoint," *IEEE Trans. Power Syst.*, vol. 31, pp. 5163-5171, 2016.
[20] P. M. Anderson and A. A. Fouad, *Power System Control and Stability*. Ames, IA: Iowa State Univ. Press, 1977, pp. 70-73.
[21] U. Rudez and R. Mihalic, "Analysis of underfrequency load shedding using a frequency gradient," *IEEE Trans. Power Del.*, vol. 26, no. 2, pp. 565-575, Apr. 2011.
[22] H. Ahmadi and H. Ghasemi, "Security-constrained unit commitment with linearized system frequency limit constraints," *IEEE Trans. Power Syst.*, vol. 29, no. 4, pp. 1536-1545, Jul. 2014.
[23] U. Rudez and R. Mihalic, "Monitoring the first frequency derivative to improve adaptive underfrequency load-shedding schemes," *IEEE Trans. Power Syst.*, vol. 26, no. 2, pp. 839-846, May 2011.
[24] F. Milano and A. Ortega, “Frequency divider,” *IEEE Trans. Power Syst.*, vol. 32, no. 2, pp. 1493–1501, Mar. 2017.
[25] B. Wang and K. Sun, "Formulation and characterization of power system electromechanical oscillations," *IEEE Trans. on Power Syst.*, vol. 31, no. 6, pp. 5082-5093, Nov. 2016.
[26] H. Saadat, *Power system analysis*, McGraw-Hill, Boston, 1999, pp. 535.
[27] “Balancing and frequency control,” NERC Resources Subcommittee, Princeton, NJ, USA, Tech. Rep. Jan. 2011, pp. 38.
[28] J. F. Restrepo and F. D. Galiana, "Unit commitment with primary frequency regulation constraints," *IEEE Trans. Power Syst.*, vol. 20, no. 4, pp. 1836-1842, Nov. 2005.
[29] F. Milano. (Mar. 2006). Power system analysis toolbox documentation for PSAT version 2.0.0_1. [Online]. Available: http://faraday1.ucd.ie/psat.html.
[30] H. Huang and F. Li, "Sensitivity analysis of load-damping characteristic in power system frequency regulation," *IEEE Trans. Power Syst.*, vol. 28, no. 2, pp. 1324-1335, May 2013.
[31] H. Golpira and A. R. Messina, "A center-of-gravity-based approach to estimate slow power and frequency variations," *IEEE Trans. Power Syst.*, vol. 33, no. 1, pp. 1026-1035, Jan. 2018.
[32] X. Fang, Q. Hu, F. Li, B. Wang, and Y. Li, "Coupon-based demand response considering wind power uncertainty: a strategic bidding model for load serving entities," *IEEE Trans. Power Syst.*, vol. 31, no. 2, pp. 1025-1037, Mar. 2016.
[33] Y. Zhang, K. Tomsovic, *et al.*, "Hybrid controller for wind turbine generators to ensure adequate frequency response in power networks," *IEEE J. Emerging and Selected Topics in Circ. and Syst.*, vol. 7, no. 3, pp. 359-370, Sept. 2017.
[34] W. Ju, K. Sun, and J. Qi, “Multi-layer interaction graph for analysis and mitigation of cascading outages,” *IEEE J. Emerging and Selected Topics in Circ. and Syst.*, vol. 7, no. 2, pp. 239-249, Jun. 2017.
[35] Y. Li, Z. Xu, and K. P. Wong, "Advanced control strategies of PMSG-based wind turbines for system inertia support," *IEEE Trans. Power Syst.*, vol. 32, no. 4, pp. 3027-3037, Jul. 2017.

Qingxin Shi (S’11), received the B.S. and M.S. degrees in Zhejiang University, China, and University of Alberta, Canada, in 2011 and 2014, respectively. He is currently pursuing the Ph.D. degree in University of Tennessee, Knoxville, USA. His research interests include demand response and dynamic demand control for system frequency regulation.

Fangxing Li (S’98–M’01–SM’05-F’17) also known as Fran Li, received the B.S.E.E. and M.S.E.E. degrees from Southeast University, Nanjing, China, in 1994 and 1997, respectively, and the Ph.D. degree from Virginia Polytechnic Institute and State University, Blacksburg, VA, USA, in 2001. Currently, he is the James McConnell Professor at The University of Tennessee (UT), Knoxville, TN, USA.

His research interests include renewable energy integration, demand response, power markets, power system control, and power system computing.

Hantao Cui (S’13) received the B.S. and M.S. degrees in Southeast University, China, in 2011 and 2013, respectively. He is currently working as a Research Associate with CURENT, University of Tennessee, Knoxville, where he is pursuing the Ph.D. degree. His research interests include energy storage systems, demand response, and large-scale power system simulations.